Available online at www.sciencedirect.com
ScienceDirect
International Journal of Pharmaceutics 324 (2006) 116–127
INTERNATIONAL JOURNAL OF PHARMACEUTICS
www.elsevier.com/locate/ijpharm

An experimental/computational approach for examining unconfined cohesive powder flow

AbdulMobeen Faqih [a], Bodhisattwa Chaudhuri [a], Albert W. Alexander [b], Clive Davies [c], Fernando J. Muzzio [a], M. Silvina Tomassone [a,*]

[a] *Department of Chemical and Biochemical Engineering, Rutgers University, United States*
[b] *Astrazeneca Pharmaceuticals LP, Wilmington, DE, United States*
[c] *Institute of Technology and Engineering, Massey University, Palmerston North, New Zealand*

Received 23 November 2005; received in revised form 28 May 2006; accepted 29 May 2006
Available online 23 June 2006

Abstract

This paper describes a new method to quantitatively measure the flow characteristics of unconfined cohesive powders in a rotating drum. Cohesion plays an important role, affecting flow properties/characteristics, mixing rates, and segregation tendencies. The method relies on measuring the change in center of mass of the powder bed as it avalanches in the vessel, using a load cell that is sampled continuously. Filtering and analysis of the signal is done using Fast-Fourier transform into the frequency domain, where noise is eliminated using signal processing methods. The filtered data is transformed back to the time domain by using an inverse Fast-Fourier transform to give quantitative information on the powder flow characteristics. In order to understand the nature of the forces controlling powder flow behavior, a computational model was developed to estimate the relationship between inter-particle cohesive strength and experimental measurements. A "flow index" generated by the method correlates well with the degree of bed expansion (dynamic dilation) of the cohesive powders. The flow index also predicts the dynamics of flow through hoppers. As the flow index increases it becomes increasingly difficult for the powder to flow through the hoppers.

Keywords: Powder flow; Cohesion; Powder avalanche; Simulations

1. Introduction

Reliable flow of particulate solids or powders from storage devices is of prime concern, among others, in agriculture, ceramic, food, mineral, mining and pharmaceutical industries. Knowledge of powder flow properties is very important when developing powder processes and handling procedures such as flow from hoppers and silos, transportation, mixing, compression and packaging (Peleg, 1978; Knowlton et al., 1994). Powder materials available in nature and industry are substantially cohesive. In many instances, this cohesive nature causes difficulties in powder flow. Cohesion-controlled flow determines whether the large majority of technologically important powders will fluidize, cake, flow out of hoppers and blenders, fill small cavities in compression and encapsulation systems, mix, or segregate.

Despite recent advances to characterize cohesive systems, flow behavior of cohesive materials is poorly understood. Majority of the academic work has focused on modeling cohesion in the engineering community by adding moisture to the system (Adams and Perchard, 1985; Lian et al., 1993; Bocquet et al., 1998; Mikami et al., 1998; McCarthy et al., 2001). Powder flow characteristics are commonly investigated under gravity loading conditions. The compressibility of a powder is a commonly used indicator of flowability and is often expressed using the Hausner ratio, which is the ratio between the tapped and the loose-packed bulk densities of the powder (Hausner, 1967). Compressibility is also one of the tests proposed by (Carr, 1965) for the assessment of powder properties. Another commonly used flow indicator is the time it takes for powder to flow out of a funnel with a standard orifice size (Staniforth, 2002). Such measurements have demonstrated the dependence of powder flowability on particles shape and size distribution (Carstensen, 1974) and on external variables such as temperature and relative humidity.

* Corresponding author. Tel.: +1 732 445 2972; fax: +1 732 445 2581.
E-mail address: silvina@soemail.rutgers.edu (M. Silvina Tomassone).

0378-5173/$ – see front matter © 2006 Elsevier B.V. All rights reserved.
doi:10.1016/j.ijpharm.2006.05.067

During the last 30 years a variety of methods for assessment of powder flow have been developed. The most common method is the shear tester in which the force required to shear a powder under well-defined conditions is measured. Shear cells can be classified into two types. The first type comprise of methods that observe the flow behavior of granular materials in its consolidated state. Besides the Jenike tester (Jenike, 1964), some other commonly used shear testers include the ring shear testers (Schulze, 1994), the Johanson Indicizers (Johanson, 1992, 1993), uniaxial, biaxial, and triaxial testers (Maltby and Enstad, 1993; Maltby, 1993), Jenike and Johanson's Quality Control Tester and some recently developed ones by SciTec (shearscan) and I-shear (E&G Associates). An extensive review on shear testers has been presented by (Schwedes and Schulze, 1990) where he also provides a comprehensive list of possible shear principles and shear testers.

No doubt, shear testers have served very successfully as an engineering tool for the design of silos for flow, and work very well for determining incipient failure conditions of soils. However, no single test is accepted as the standard. Besides, the experimental determination of a flow function is time-consuming and it is difficult to achieve reproducibility for cohesive powders due to the powders ability to consolidate differently.

The second type consists of methods that correlate flow properties to flowability in a loose dilated state. Such methods consist of static and dynamic angle of repose, discharge time under standard conditions, fluidization degree and powder deaeration rates. In fluidization methods, the most widely used classification system for particles in two-phase flows was introduced by (Geldart, 1973) based on the density difference between the particles and the fluid and the average particle diameter—where particles are considered cohesive (C), aeratable (A), sandlike (B) and spoutable (D) as particle diameter increases. However, the first principle basis for the group boundaries and their variation as a function of interparticle force is unclear.

As mentioned above, the angle of repose is often used to characterize flowability. Independent of the specific method the procedure is always similar. Bulk solid flows onto a flat surface and forms a pile. As soon as the pile is formed, fresh bulk solid flows erratically along the pile surface in the form of avalanches. The way the avalanches are formed, their size, and frequencies strongly depend on the flowability of the bulk solid.

The dynamics of avalanching behavior of bulk solids has been investigated by many authors (Bagnold, 1941; Brown and Richards, 1960; Savage and Hutter, 1989; Rastogi and Klinzing, 1994; Koeppe et al., 1998). Most previous studies focusing on avalanches in laboratory scales have relied on direct observation of the granular flow in transparent short cylindrical drums with a small length-to-diameter ratio (Quintanilla et al., 2001; Takeuchi et al., 2003). While such systems produce a great deal of interesting information, the effect of the walls in such systems is often a concern. In this article, we build on a proposed concept by (Kaye et al., 1995), where he characterizes the avalanching behavior of powders by using a photovoltaic array in a narrow disk partially filled with powder. This device has been patented and commercialized under the name "Aero-Flow". Even though the basic concept of the device is sound, several shortcomings have been identified. The narrowness of the disk makes the particle–wall friction significant, which is rarely the case in industrial mixers. Since wall effects become larger as the cylinder diameter increases, the device is unsuitable for scale-up and is limited to free-flowing powders. Also, insufficient modeling has been conducted, relating the measurement (fluctuating torque signal) to true material property.

The rotating drum is the simplest of all tumbling blenders and provides a constant influx of energy into the system because the blender is perfectly symmetric with respect to the rotation axis (unlike other blenders such as the v-blender, bin blender, or double cone). A wide variety of flow regimes, including periodic motion, weakly chaotic motion, and strongly chaotic flow, are observed for different cohesive materials perturbed by different experimental conditions (vessel speed, fill level, tumbling time). Here, in the interest of brevity, we focus on the analysis of the relationship between inter-particle forces and the observed avalanching phenomenon, which was further explored by using a numerical discrete element models (DEM) (Cundall, 1971; Strack and Cundall, 1979). In the experiments, the quantification scheme relies on measuring the change in the center of mass of the powder bed due to avalanches using a load cell that is placed below the vessel and is sampled continuously. Filtering and analysis of the resultant signal gives quantitative information on the flow characteristics of the material within the vessel.

This paper communicates a new method for characterizing the flow properties of cohesive powders under unconfined conditions, i.e., where the cohesive powder is in a dilated state. The methodology uses the concept of the change in center of mass of the system as the avalanche cascades and that the magnitude of the avalanche is directly proportional to the cohesion of the material. A flow index is defined, which helps in correlating powder cohesion to dilation of the powder bed and also to understand the dynamics of flow through bench scale hoppers.

2. Materials

We used well-characterized powder systems of varying cohesion. The materials used in our experiments are presented in Table 1.

3. Experimental setup and method

A new devise, called the gravitational displacement rheometer (GDR) was developed to quantitatively measure the flow characteristics of cohesive powders in a rotating drum. The appa-

Table 1
Materials used with corresponding size and degree of cohesiveness

Pharmaceutical material	Size and morphology	Vender, City, State
Fast-Flo lactose	~100 μm, spherical	Foremost farms, Newark, NJ
Avicel 102	~90 μm, needle-like	FMC, Rothschild, WI
Avicel 101	~60 μm, needle-like	FMC, Rothschild, WI
Milled lactose	~50 μm, irregular shape	Foremost farms, Newark, NJ
Glass bead	~700 μm, sphere	Potter Industries, Carlstadt, NJ

ratus employs a long cylinder to minimize wall effects and uses a load cell to measure changes in the center of gravity that are correlated to specific powder flow behavior. A schematic of the GDR is shown in Fig. 1. The cylinder and its drive mechanism are mounted on a pivoted framework which acts on a load cell. The basic idea is that an avalanche will move a portion of the material down the cascading surface. This displacement will change the center of mass of the powder within the cylinder, which can be measured by the force registered by the load cell. The size and frequency of these slumps can be then assessed and used to characterize the cohesion of the material.

The GDR has evolved gradually over two years into a robust technique for analyzing flow properties of granular materials. A photograph of the apparatus is shown in Fig. 2a. The unit consists of a cylinder, measuring 8 in. in diameter and 10 in. deep. The entire cylinder is constructed of a transparent Plexiglas, which allows for observation of the dynamics within the blender, even though transparency is not necessary for data acquisition. Furthermore, video imaging may be used to directly relate the data output to specific movements of the powder within the vessel. The drive train is a 130 V DC motor by Glas-col (Terre Haute, IN, in USA) with a maximum speed of 2500 rpm and an output of 190 W. This motor was connected to the system using a flexible drive shaft, and the cylinder was held in place by spring loaded pins (not shown). The data was acquired for speeds from 5 to 30 rpm to capture the relevant dynamics of flow. The load cell used in this work was a 5 lb subminiature compression load cell, type 13/2443-06 by Sensotec, Ohio, USA. The range of the load cell determines the sensitivity of the experiment. The deadweight of the drive assembly and framework can be reduced to any required level by an adjustable counterweight. This allows in principle the absolute range of the load cell to be significantly lowered, increasing the overall sensitivity of the instrument. For the scale used here, a 5 lb load cell provides optimal conditions to detect the change in center of mass across the cylinder.

In all experiments, the cylinder was loaded with powder to approximately 40% by mass and rotated at the selected speed, and the load cell is sampled at a frequency of 2000 Hz for 100 s. The data collection is begun approximately 5 min after the cylinder is first started in order to get the steady-state data and ignore the initial transient phase in which avalanches are noticeably larger due to the initial tensile cracking phenomena. The 5 min conditioning time is a precautionary step and is representative of the time it takes for the most cohesive powder to reach steady state. Comparison of the time-series obtained from experiments show that 5 min is indeed enough to achieve steady state. Once steady state is achieved the impact of conditioning time is no longer relevant as the powder properties within the system remain unchanged. The high frequency allows in eliminating noise caused due to vibrations by external sources. Considerable effort was focused on the development of the data analysis tools, aimed at minimizing noise in the system. A custom program was developed to evaluate the Fast-Fourier transform of the data set and plot the power spectrum discussed in the next section.

Many industrial applications involve powder flow through funnels or hoppers. One of the major industrial powder problems is obtaining reliable and consistent flow out of hoppers. It

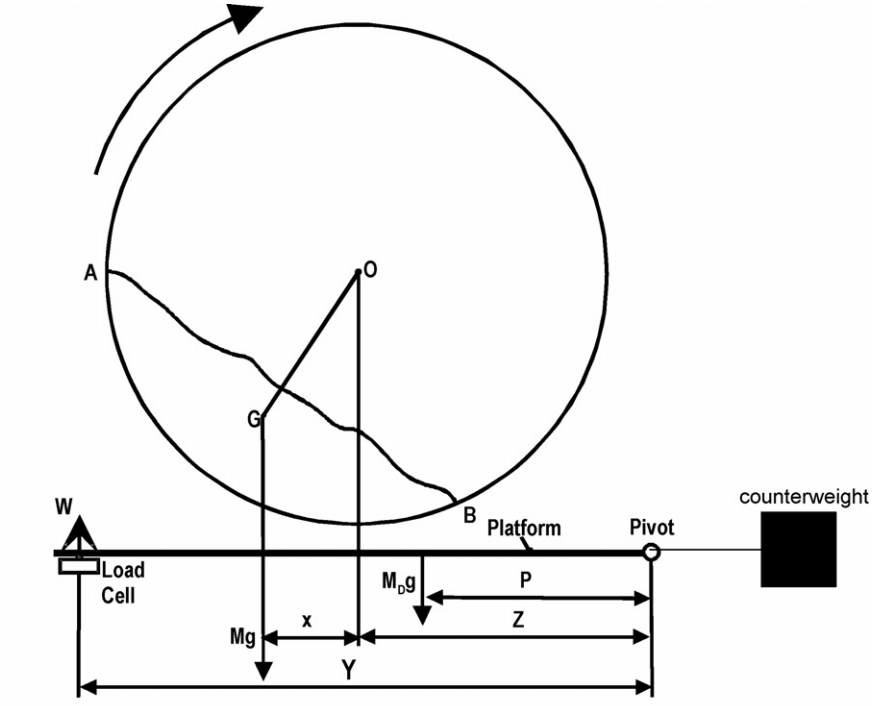

W – weight on the load cell; 'O' – center of the cross-sectional area of cylinder; '
x' – distance between center of Cylinder and center of the powder bed 'G';
'Z' – distance between the center of the cylinder and the pivot.

Fig. 1. A Schematic showing moments of material in cylinder system deadweight, and load cell reaction.

is shown that the flow index obtained by GDR measurements can be used to evaluate flow in a hopper of varying angle at fixed temperature and moisture conditions, providing a predictive method for hopper design and a convenient experimental test for screening materials and determining their suitability for specific hopper systems. The powder discharged from the GDR is transferred into a set of hoppers of five different angles (35°, 45°, 55°, 65°, and 75°) bored out of solid Plexiglas cylinders to simulate industrial conditions (Fig. 2b). As mentioned by Nedderman et al. (1982) the angle measured was at the exterior of the hopper with respect to the horizontal plane shown in the figure. Removable opening sections were built in order to be able to adjust the diameter of the discharge of the steepest hopper (0.5–1.0 in.).

3.1. Data collection and analysis

The load cell output is a continuous analog signal that is digitally sampled through a computer interface. In order to get adequate precision in the frequency domain, it was decided to sample the signal at 2000 Hz. Samples were taken over 100 s

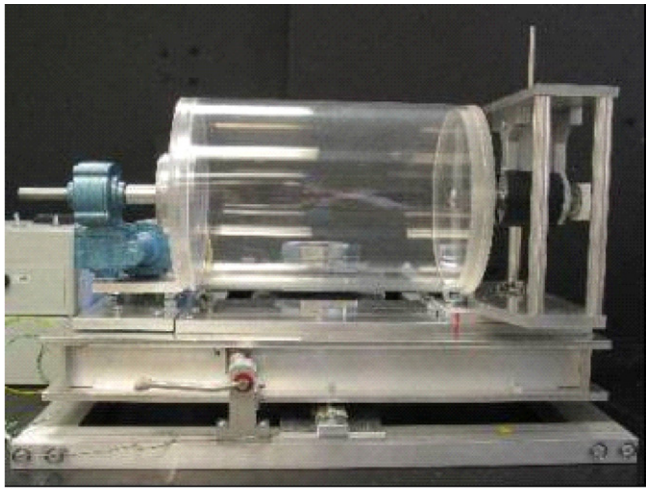

(a)

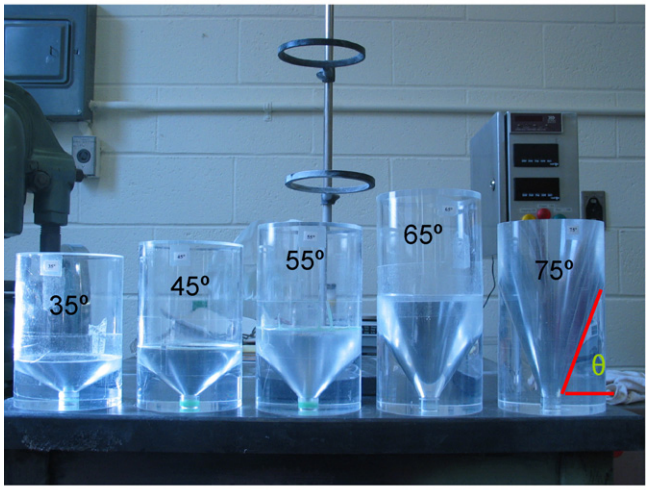

(b)

Fig. 2. (a) Picture of the apparatus showing the vessel, drive and load cell. (b) A picture of the Hopper setup with varying angles ranging from 35° to 75°.

and then, using a Fast-Fourier algorithm, data were transformed into the frequency domain. An example of the raw time-series data and the power spectrum of the transformed data is shown in Fig. 3 for the four powders at 15 rpm. The raw data is a time series of variations in measured weight as the cylinder rotates (and the mixture tumbles). In order to compare materials with different densities, it is necessary to divide the weight data by the density of the material to get "volume" data which is directly comparable for different materials. Generally, as materials become more cohesive, the amplitude of the signal increases. This is a general indication of larger avalanches. However, as seen in Fig. 3c and d, Avicel PH101, which has smaller avalanches, has greater amplitude than the regular lactose, which has larger avalanches. The reason for this apparent discrepancy is that the amplitude of the signal is the difference between the minimum and maximum weight supported by the load cell. The device only measures displacement of the center of mass of the material, not the size of individual avalanches. Regular lactose has larger avalanches than Avicel PH101, however, because Avicel flows "better", it goes through more extreme changes in the shape of the flowing layer, i.e., the avalanche travels further and, hence, changes in center of mass. This difference is demonstrated in Fig. 4, where the relative change in the shape of the flowing layer in each frame following the first for each set shows more variation in the Avicel system than the lactose system. These results indicate that interpretation of data has to be tempered with visual analysis of the flow; otherwise incorrect conclusions can be drawn.

The first step in the data analysis is to evaluate the Fast-Fourier transform of the data set and plot the power spectrum versus frequency. The power spectrum for the data stream from Fig. 3 is shown in Fig. 5a, spanning from 0.1 to 200 Hz. A number of different peaks are observable in the power spectrum near 2, 20, 180 Hz. As mentioned earlier, the goal of this methodology is to measure the change in measured weight that is caused by avalanching behavior of the granular material within the cylinder. Observation of the mixture flow dynamics indicates that avalanching occurs at a frequency in the range of 1–5 Hz depending on the rotation rate of the cylinder. We expect meaningful data to be found over that frequency range shown in Fig. 5b.

In order to test the hypothesis that the useful data is found near 1–5 Hz, two trials were run for comparison; one with an empty cylinder and the other with the cylinder filled with large (∼700 μm) glass beads, which are completely free-flowing. In both of these experiments, there was little or no signal in the 1–5 Hz region. The reason is obvious for an empty cylinder. For glass beads, there should be little or no 'avalanching' behavior because there is no cohesion between particles and, hence, individual particles move independently, not as large avalanche events. Representative data output and power spectrum for both experiments are shown in Fig. 5c for the empty cylinder and glass beads. For the empty cylinder, there are three large peaks in the data, near 0.1 Hz, near 20 Hz and near 180 Hz. The peak near 0.1 Hz is caused by imperfections in the cylinder that cause a periodic component in the data stream once every 0.5 revolutions (think of the generation of a wobble by gluing a steel ball to the outside of the cylinder). The peak at 180 Hz is vibrational noise and the peak near 20 Hz is the natural oscillation

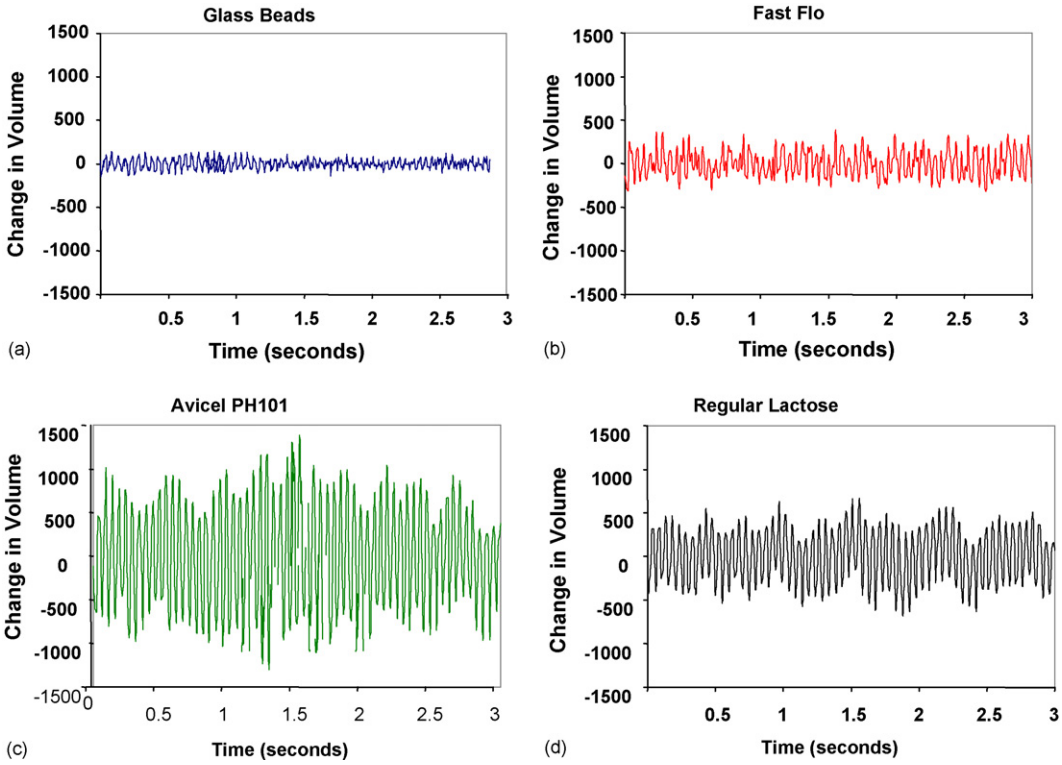

Fig. 3. The data from the GDR after division by the powder density and subtraction of the mean to allow direct comparisons of the four materials. The figures correspond to the images shown in this figure: (a) glass beads, (b) Fast-Flo lactose, (c) Avicel PH101, and (d) regular lactose.

frequency of the damped oscillator that defines this system. The close up over the range of 0.1–5 Hz shows only the one peak coming from the cylinder.

For the glass bead experiment, there are also three large peaks in the power spectrum, along with multiple smaller peaks. The peak near 20 Hz is the spring oscillator associated with the load cell, and the one near 180 Hz is similar noise as seen in the empty cylinder. In the range of 0.1–5 Hz, there is a scattering of small peaks, but not much organization when compared to the data from Fig. 5b for the lactose. The scattered signal in this range for the glass bead data indicates that there is some minor avalanching-like behavior taking place but that it does not occur regularly (hence the lack of organization or significant peaks).

Hence, it appears that for cohesive powders the useful data will be found over the range of ∼0.1–5 Hz (this range can change depending on rotation rate) and the ensuing discussion will focus on data taken over this range of frequencies. The evidence that the useful data is found over this range of frequencies is further enhanced by examining the data from Fast-Flo Lactose in Fig. 5d. The data in the range of ∼0.1–5 Hz is much more organized and much stronger in power than seen for the glass bead data, but weaker than regular lactose. This revelation emphasizes that avalanching data that is crucial to the measurement of cohesive materials can be found in this range. Similar to the previous data, there are peaks near 20 Hz, although the relative strength of this peak varies widely from experiment to experiment. The chosen frequency domain (0.1–5 Hz) was then transformed back to the time domain using inverse Fourier transform (this procedure is demonstrated in Fig. 6). The unfiltered data for regular lactose is shown first (blue) and is compared with the filtered data on the same scale (red).

Once the data has been transformed back into the time domain, the variance of the filtered time-series data gives a quantitative value of the change in center of mass for that set of experimental conditions (powder type, rpm, fill level, etc.). Different materials are characterized and compared by taking data over a range of rotation rates and comparing the quantitative changes in variance. As shown by simulations in Section 4, the variance of the signal is proportional to cohesion. Typically, higher variances will correspond to large changes in the center of mass/volume (avalanching) and is indicative of strong avalanching which is associated with cohesive materials.

3.2. Variations with rotation rate

As the rotation rate is increased, and, hence, the energy input and the rate of mass flow is increased, we expect the material to undergo changes in both the frequency and power of the avalanches. Fig. 7 shows that for regular lactose the variance increase up through 20 rpm, as the avalanches become larger, accompanied by a strong pulsing behavior. The pulsing behavior can be followed by observing the signal. As the rpm increases, the amplitude and frequency of the signal changes from weak, non-periodic oscillation to strong and highly periodic. As the rotation rate further increases, material reacts to higher energy/mass input by creating more frequent avalanches. At this point, it is experimentally observed that individual avalanches traverse on top of one another and the periodic beat-

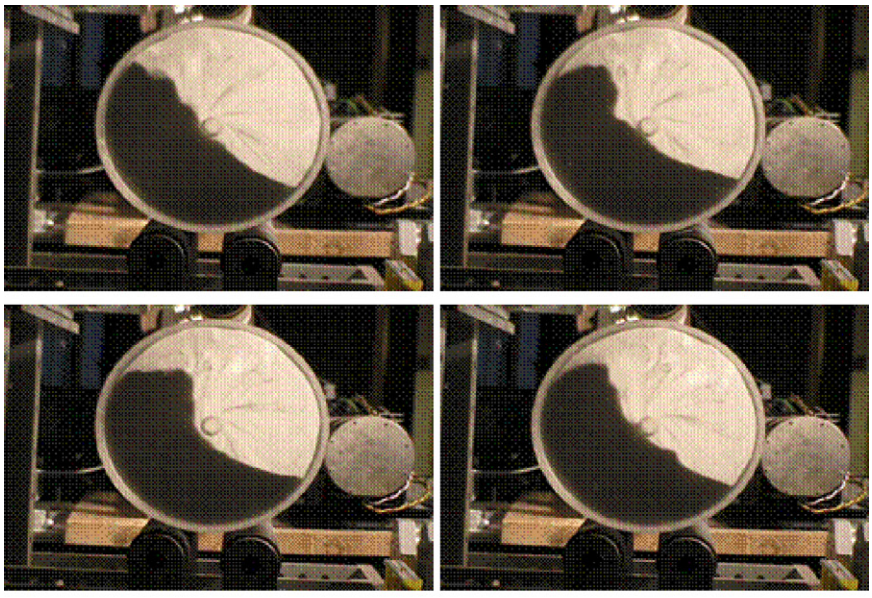

(a) Frame #: 37-49-63-77, 29.97 fps

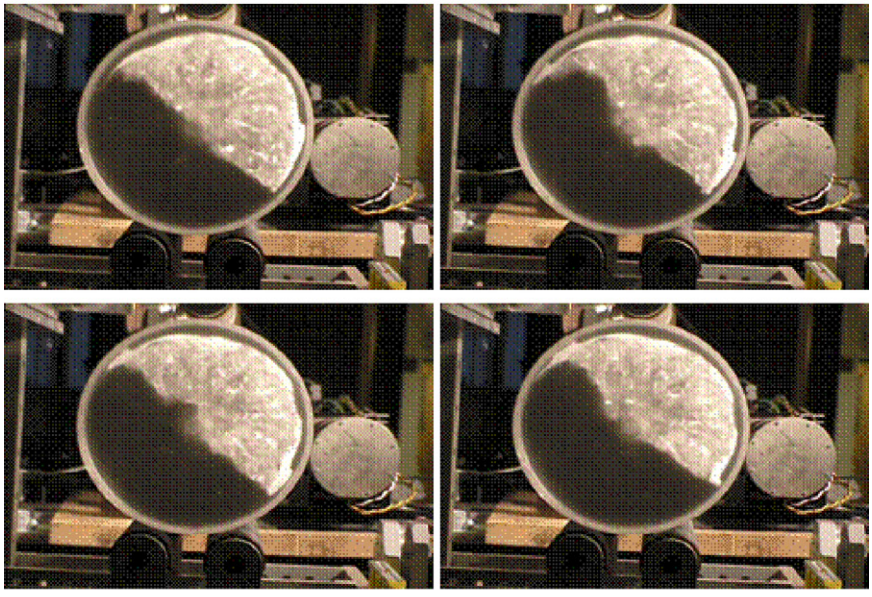

(b) Frame #: 65-77-85-90, 29.97 fps

Fig. 4. Stills taken at various times for (a) Avicel PH101 and (b) regular lactose which demonstrate that the Avicel, even though it has smaller avalanches, goes through more extreme variation in change in center of mass and, thus, has a stronger signal than the regular lactose.

ing that was observed at lower rotation rates is destroyed. The frequency continues to increase because there are more changes per unit time in the center of mass of the material even though the organized structure of the deformations has been eliminated. This decrease is an indication of a change in flow behavior that is likely to be important in regards to mixing or segregation phenomena in tumbling blenders.

4. Numerical model

The discrete element method (DEM), originally developed by (Cundall, 1971; Strack and Cundall, 1979), has been successfully used to simulate chute flow (Dippel et al., 1996), heap formation (Luding, 1997), hopper discharge (Thompson and Grest, 1991; Ristow and Herrmann, 1994) and flows in rotating drums (Ristow, 1996; McCarthy and Ottino, 1998; Wightman et al., 1998). In our present study we use DEM to simulate the dynamic behavior of cohesive and non-cohesive powder in a rotating drum. We consider the granular material as a collection of frictional inelastic spherical particles. Each particle may interact with its neighbors or with the boundary only at contact points through normal and tangential forces. The forces and torques acting on each of the particles are calculated in the following way:

$$\sum F_i = m_i g + F_{\mathrm{N}} + F_{\mathrm{T}} + F_{\mathrm{cohes}} \quad (1)$$

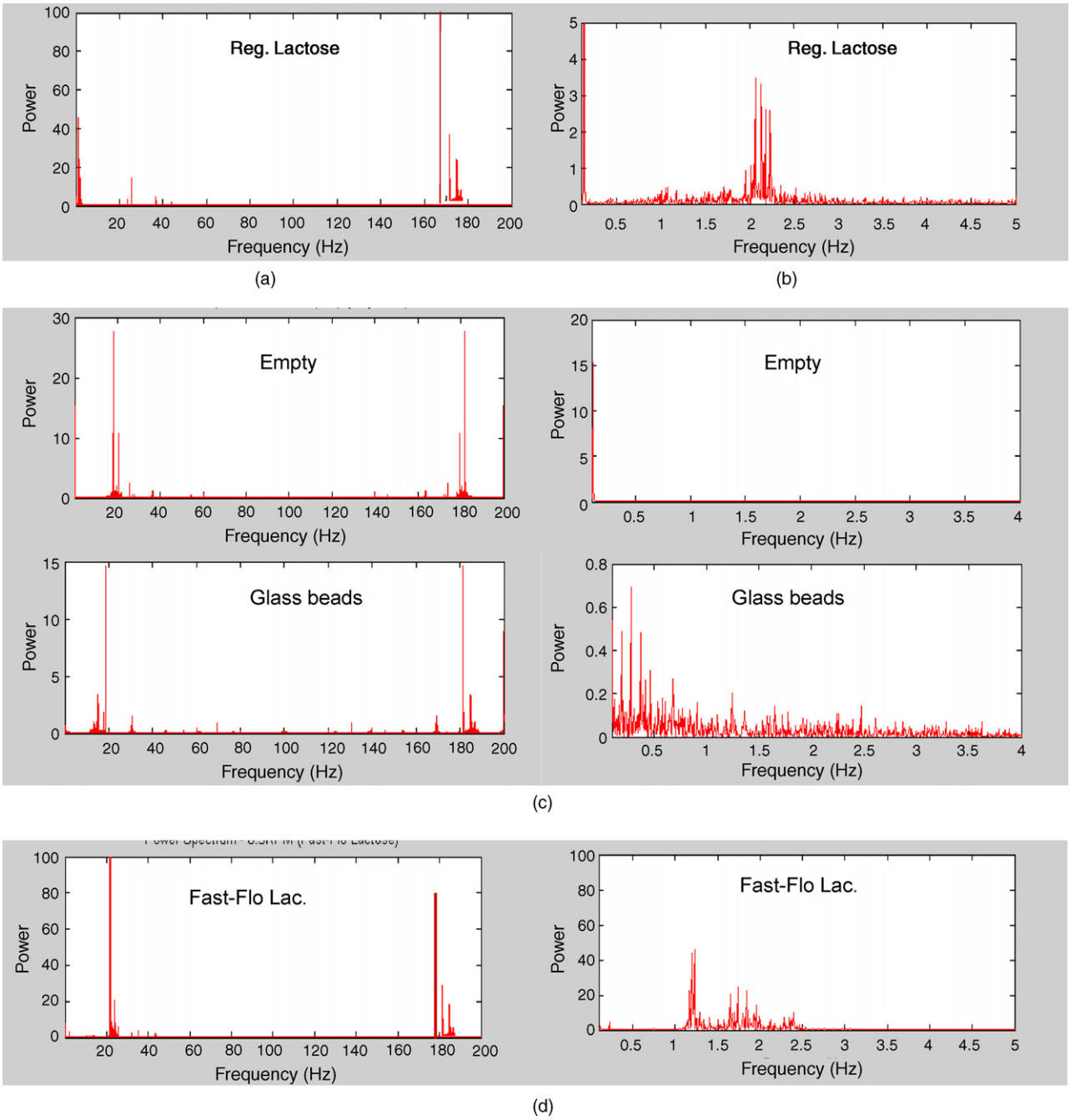

Fig. 5. Power spectrum for regular lactose at 15 rpm over 200 Hz (a); over 5 Hz (b); power spectrum for empty cylinder and glass beads for comparison (c); Fast-Flo lactose shows the presence of peaks between 0.1 and 5 Hz confirming the importance of the region (d).

$$\sum T_i = r_i F_T \tag{2}$$

The force on each particle is given by the sum of gravitational, interparticle (normal and tangential F_N and F_T) and cohesive forces as indicated in Eq. (1). The corresponding torque on each particle is the sum of the moment of the tangential forces (F_T) arising from inter-particle contacts (Eq. (2)).

The normal forces are calculated with the "latching spring model", developed by (Walton and Braun, 1986; Walton, 1992, 1993), which allows colliding particles to overlap, and the corresponding interaction force (normal force) is a function of this relative overlap. Each particle may interact with its neighbors or with the boundary only at contact points through normal and tangential forces. The normal forces between pairs of particles in contact are defined using a spring with constants K_1 and K_2 for compression and recovery: $F_N = K_1\alpha_1$ (for compression), and $F_N = K_2\ (\alpha_1 - \alpha_0)$ (for recovery). These spring constants K_1 and K_2 are chosen to be large enough to ensure that the overlaps α_1 and α_0 remain small compared to the particles sizes. The degree of inelasticity of collisions is incorporated in this model by including a coefficient of restitution $e = (K_1/K_2)^{1/2}$ $(0 < e < 1$, where $e = 1$ implies perfectly elastic

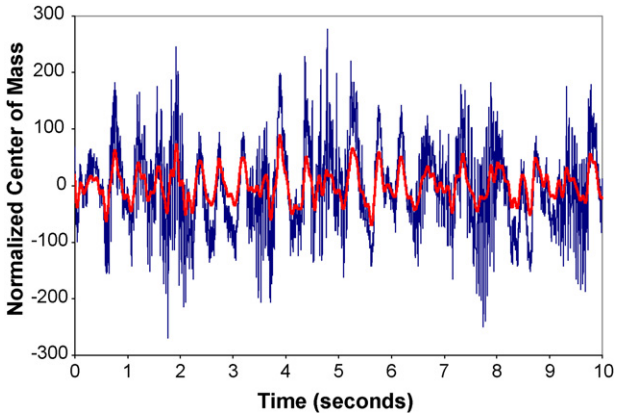

Fig. 6. For regular lactose run at 16 rpm, the raw data in blue, filtered data in red. The filtering process cleans up the raw data and gives a good indication of the changes (avalanches) occurring as the cylinder rotates. (For interpretation of the references to colour in this figure legend, the reader is referred to the web version of the article.)

collision with no energy dissipation, $e = 0$ implies completely inelastic collision).

Tangential forces (F_T) in inter-particle or particle–wall collision are calculated employing Walton's incrementally slipping model. After contact occurs, tangential forces build up, causing displacement in the tangential plane of contact. The initial tangential stiffness is considered a fraction of the normal stiffness. Proper definition of frictional forces proved to be exceedingly important in obtaining an accurate model. In all cases, the static frictional limit was considered to follow Coulomb–Amontons's law, i.e., if $F_T \leq \mu_S F_N$ (μ_S is the static friction coefficient and F_N is the total normal force, equal to the cohesive force plus the static weight of particles transmitted through the bed), no relative motion between particles occurred, while if the particles are in relative motion with respect to one another, $F_T = \mu_D F_N$, where μ_D is the dynamic friction coefficient. This model takes into account the elastic deformations that can occur in the tangential directions of the contacts. The tangential force T is evaluated considering an effective tangential stiffness k_T associated with a linear spring. It is incremented at each time step as $T_{t+1} = T_t + k_T \Delta s$, where Δs is the relative tangential displacement between two time steps (Walton, 1993). The described model has been successful to obtain the first three-dimensional computations of realistic blender geometries, where it confirmed important experimental observations (Wightman et al., 1998; Shinbrot et al., 1999; Moakher et al., 2000; Sudah et al., 2005).

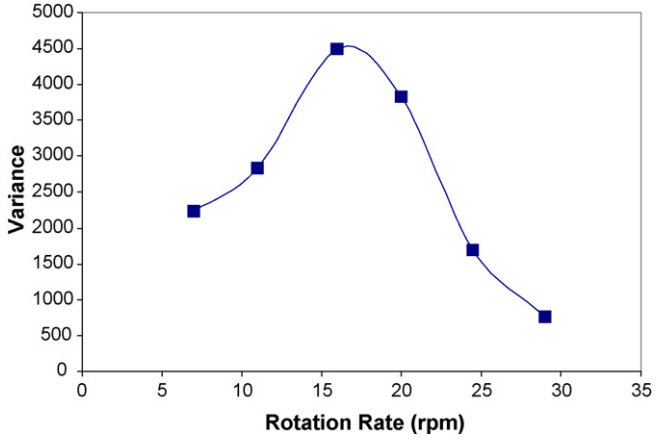

Fig. 7. The change in variance with increasing rotation rate for regular lactose. There is an indication of a change in flow dynamics as the rotation rate is change from 16 to 20 rpm.

To incorporate granular cohesion in the model, a cohesive force between particles is simulated using a square-well potential. Two parameters are needed to define the square well: the well width r (equal to the radius of the particle) and the well depth K. The cohesive interactions arise when the separation distance of two particles is less or equal to twice the width of the square well ($2r$). In dimensionless terms, in order to compare simulations considering different numbers of particles, the magnitude of the force was represented in terms of the parameter $K = F_{cohes}/mg$, where K is called the Bond number and is a measure of cohesiveness that is independent of particle size, F_{cohes} is the cohesive force between particles, and mg is the weight of the particles. Notice that this constant force may represent short range effects such as electrostatic or van der Waals forces. In this model, the cohesive force (F_{cohes}) between two particles or between a particle and the wall is unambiguously defined in terms of K. Four friction coefficients are also defined: particle–particle static and dynamic coefficients, and particle–wall static and dynamic coefficients. Interestingly, all four-friction coefficients turned out to be important. To emulate different levels of cohesion, the bond number K, the coefficients of static and dynamic friction between particles (μ_{SP} and μ_{DP}) and the coefficients of static and dynamic friction between particle and wall (μ_{SW} and μ_{DW}) are varied.

The major computational tasks of DEM in each time step are as follows: (i) add/delete contact between particles thus updating neighbor lists, (ii) compute contact forces from contact properties, (iii) sum all forces and torques on particles and update position and (v) determine the trajectory of the particle by integrating Newton's laws of motion (second order scalar equations in three dimensions). A central difference scheme, Verlet's Leap Frog method is used here.

5. Results

The quantification experimental and computational method described above enables us to document the flow properties of different materials by calculating the variance or standard deviation of the center of mass at varying rotation rates.

5.1. Effect of cohesion

Typical results of this methodology are shown in Fig. 8. The figure shows the standard deviation (S.D.) of the weight signal as a function of drum speed (measured in rpm) for five materials (glass beads, Fast-Flo lactose, Avicel 101, Avicel 102, regular lactose). For most of the powders, as drum speed increases, the size of avalanches also increases due to the effect of the centrifugal forces, which add themselves to the frictional–cohesive forces in resisting the onset of avalanches. However, at even higher speeds, the rate of avalanche formation increases while

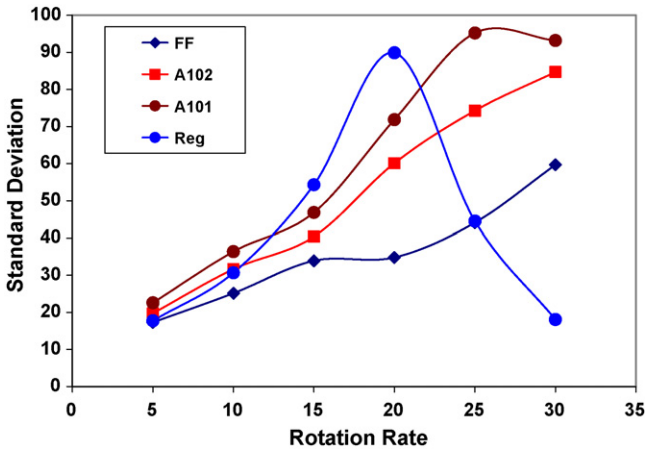

Fig. 8. Standard deviation as a function of the vessel speed. As dry cohesion increases the R.S.D. increases; glass beads is almost a flat profile.

their mean lifetime stays constant. As a result simultaneous avalanches occur and the S.D. of the signal goes through a maximum, and then decreases as avalanches begin to overlap. As a consequence of this overlap, there is not enough time resolution to capture an appreciable change in the weight signal, causing a decrease in the standard deviation of the powder weight. The basic observation is that the magnitude of avalanches grows consistently as the powder becomes more cohesive. This observation constitutes the conceptual basis of the technique used in this article to characterize flow properties of unconfined (dilated) powders.

It is also interesting to note that the experiments were performed at 45% RH and 75 °F. At this condition static charges that develop for the four powders in a plastic cylinder are fairly insignificant. The experiments were also performed using a metal cylinder showed similar results indicating that the material of construction for the cylinder is not an essential factor. Electrostatics can play a role under other conditions. Such effects will be a part of a future communication.

The GDR measurement is supplemented by direct observation of powder flow behavior. Fast-Flo lactose, a mildly cohesive powder, exhibits weak avalanching tendencies (nearly constant streaming flow). The flowing layer (not shown) forms a crescent-like shape such that the material creates two dynamic angles of repose at the top and bottom halves of the cylinder. The variance of load cell measurement (not shown) becomes more pronounced as the rpm increases, revealing relatively bigger avalanches that travel further. Avicel PH102 exhibits larger avalanches than Fast-Flo lactose that travel continuously to the end of the cylinder. The larger avalanches result in a higher variance. For Avicel PH101, the avalanches are much larger at low rotation rates. Regular lactose, the most cohesive material used in this study, forms the largest avalanches. Here the powder peaks at 20 rpm before starting to drop again. This is due to the fact that as rotation rate increases, the avalanches overlap on top of one another causing a drop in the variance. This is due to the ability of the load cell to only measure the change in center of mass and not the individual frequency of the avalanches.

5.2. Flow comparison between experiments and simulation

In order to understand the nature of the forces controlling powder flow behavior, a computational model was generated to determine the relationship between inter-particle cohesive strength and the GDR measurements. Our model system consisted of 20,000 particles of 2 mm diameter in a cylindrical vessel with a 9 cm diameter, 1 cm length, and frictionless side walls. The cohesive force between particles was simulated using a square-well potential; a constant-intensity normal force was applied whenever particles were in contact. In our model, the magnitude of the cohesive bond number K is chosen in the same order of magnitude as the ones measured with AFM by (Doung et al., 2004) and also in the numerical model of (Baxter et al., 2000). The constant K was varied between 0 and 90; for $K < 30$, no avalanches were observed, and for $K > 90$, avalanches were of magnitude comparable to the size of the system and therefore examination of larger values was unwarranted. The model displayed discrete, well-defined avalanches for the moderate and higher cohesion scenario, with a K value greater than 45. Computational parameters were fine-tuned to accurately simulate flow of the four materials. The following methods were used to validate the code: (a) direct visual comparison of the shape of the flow region, including local angles of repose, (b) size of avalanches, and (c) degree of dilation of the material. Subsequently, sets of cohesion and friction coefficients were identified that accurately matched flow behavior of Fast-Flo lactose, Avicel 102, Avicel 101, and micronized Lactose. Typical results for Fast-Flo lactose, Avicel 101 and their corresponding matching simulation snapshots are displayed in Fig. 9. A table providing the sets of simulation parameters for the four pharmaceutical materials of interest is given in Table 2.

5.3. Definition of a quantitative flow index using GDR measurements

The simulations played an essential role in the determination of a meaningful flow index capable of capturing the effect of the cohesive powder behavior. The essential assumption behind the GDR method was that the standard deviation of the load cell signal would be proportional to the intensity of cohesive interparticle forces. This assumption cannot be verified experimentally due to a lack of an independent method to measure cohesion directly under relevant (dilated) conditions. However, this assumption is easily tested computationally, where the inten-

Table 2
Comparison of simulation parameters to pharmaceutical powders

K	μ_{sp}	μ_{dp}	μ_{sw}	μ_{dw}	Pharmaceutical material
0	0.8	0.1	0.5	0.5	Glass beads
45	0.8	0.1	0.5	0.5	Fast-Flo
60	0.8	0.6	0.8	0.8	Avicel
75	0.8	0.6	0.8	0.8	Regular lactose

K: cohesion number; μ_{sp}: static friction between particles; μ_{dp}: dynamic friction between particles; μ_{sw}: static friction between particle and wall; μ_{dw}: static friction between particles.

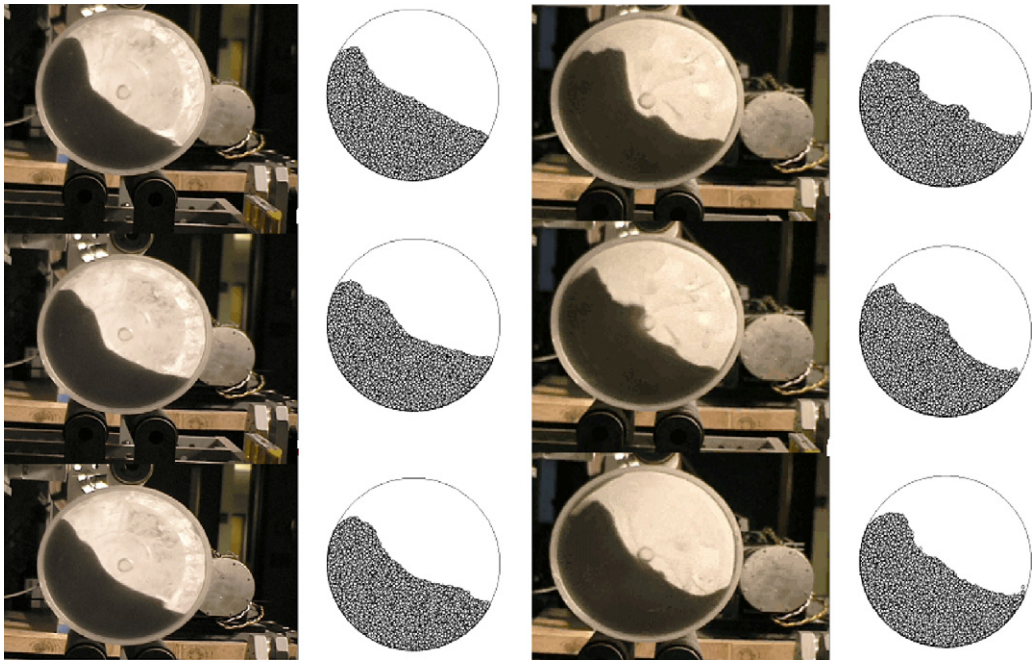

Fig. 9. (a) Shows the time sequence of axial snapshots of Fast-Flo lactose in a rotating drum. (b) Shows the simulation snapshots for $K = 45$. (c) Shows the time sequence for Avicel-101. (d) Shows the snapshots from simulation for $K = 60$.

sity of cohesive forces is know exactly (and is given by Kmg) and the moment of inertia of the particle system with respect to any point can be easily calculated. Fig. 10 shows the results of these calculations. Provided that the speed of the vessel is sufficiently slow to allow individual avalanches to flow independently from one another, a nearly linear relationship is observed between the cohesion K and the standard deviation of the moment of inertia in the entire range of cohesive forces examined here, which is wide enough to capture the behavior of materials as diverse as regular lactose and Fast-Flo lactose. In other words, simulations demonstrate that the R.S.D. of the GDR measurement is proportional to cohesion.

Given the results shown above, a flow index is easily and conveniently defined as the average R.S.D. of the load cell signal in the low (5–20) rpm range. Since the R.S.D. was measured at standard vessel speeds of 5, 10, 15, and 20 rpm, for practicality the index is defined as

$$\text{IND} = \frac{\text{R.S.D.}_{5\,\text{rpm}} + \text{R.S.D.}_{10\,\text{rpm}} + \text{R.S.D.}_{15\,\text{rpm}} + \text{R.S.D.}_{20\,\text{rpm}}}{4}$$

This quantitative flow index provides a convenient, sensitive, and practical single-number quantifier of powder flow properties under dilated conditions. An illustration of the flow index for the four materials is shown in Table 3, where increase in cohesion relates to a higher IND value.

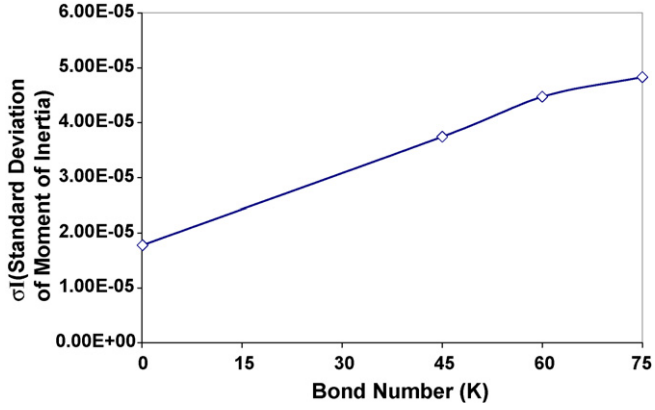

Fig. 10. Computational results demonstrating the existence of a monotonic relationship between the cohesive stress K and the standard deviation of the moment of inertia of the particle assembly.

5.4. Comparison of GDR measurement to powder dilation

In order for the powder to flow it has to dilate (expand). This phenomenon is known since it was pointed out by (Hagen et al., 1852; Reynolds, 1885). In general, also, there is a (somewhat vague) awareness that more cohesive powders dilate more extensively. In this study, a custom—designed pixel-counting program is used to determine the relative volumes of powder to void (Faqih et al., 2006). It is assumed that bed dilation is uniform along the axis of the cylinder; visual observations and snapshots along the length of the cylinder support this assumption. Analysis of pixel data is done for snapshots taken at every 0.3 s for simulations and 1 s for experiments. The initial volume

Table 3
Comparison of the flow index and degree of dilation

Pharmaceutical powders	Flow index	Dilation (% expansion)
FF lactose	27.8	11
Avicel 102	38.0	15
Avicel 101	44.4	17
Regular lactose	48.2	21

Table 4
Correlation of flow index from GDR measurement to hopper flow

Pharmaceutical powders	Flow index	35°, 0.5 in.	45°, 0.5 in.	55°, 0.5 in.	65°, 0.5 in.	75°, 0.5 in.	75°, 0.75 in.	75°, 1.0 in.
FF Lactose	27.8	FF[a]	FF	FF	MF[b]	MF	MF	MF
Avicel 102	38	NF[c]	NF	NF	IF[d]	IF	IF	MF
Avicel 101	44.4	NF	NF	NF	NF	IF	IF	MF
Regular lactose	48.2	NF	NF	NF	NF	NF	NF	NF

[a] Funnel flow.
[b] Mass flow.
[c] No flow.
[d] Intermittent flow.

of the bed at time $t = 0$ s (no rotation) is considered as $\text{volume}_{\text{initial}}$ and at any later time as $\text{volume}_{\text{new}}$. Dilation is quantified as the percent increase in bed volume relative to the initial volume. Time $t = 0$ is taken as the last frame before the onset of powder movement:

$$\%\text{increase in bed volume} = \frac{\text{volume}_{\text{new}} - \text{volume}_{\text{initial}}}{\text{volume}_{\text{initial}}}$$

The surprising result, however, was the extent of dilation exhibited by common pharmaceutical ingredients: up to 30% for lactose, and up to 100% for MgSt (please refer to dilation paper for more details). Fig. 11 shows the changes in powder dilation for the four materials from Table 1. In general, dilation increases with increase in cohesion. The values are compared in Table 3, where the IND for varying cohesion is directly related to the bed expansion. In fact, since dilation follows precisely the same monotonic order as the GDR flow index, the conclusion is that the flow index can be used to predict the degree of dilation of a material. This observation is very important since the degree of dilation reported here can easily cause a blender to become overfilled, which would in turn cause its mixing rate to plummet, possible causing the blending process to fail.

5.5. *Correlating the measurement technique to flow in hopper*

In order to demonstrate the relevance of the flow index obtained from the GDR system, a series of experiments was performed, where the materials discharged from the cylinder were run through a series of hopper of varying angle and orifice diameter. As the standard deviation (S.D.) of the GDR signal (i.e., the blend cohesion) increased, flow through hoppers became increasingly difficult. The behavior of each material in each hopper was classified according to four main behaviors: funnel flow, mass flow, intermittent flow (caused by steady vibration), and no flow. A condensed version of these results are shown in Table 1, which displays extremely convincing evidence that the flow index predicts whether a given material will or will not flow out of a given hopper.

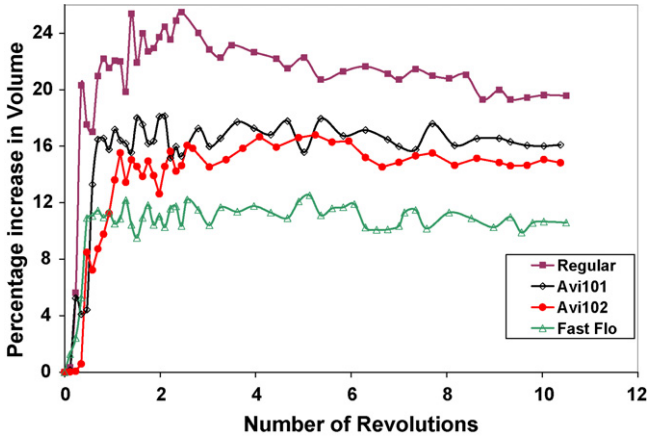

Fig. 11. The change in dilation for materials of different cohesion is shown at 7 rpm.

This correlation reflects the fact that the onset of flow in a hopper is controlled by the powder's "unconfined bridging length", which is a manifestation of the same cohesion-generated internal "flow length scale" that also controls the size of an avalanche. These results provide strong motivation to investigate further the relationship between avalanches in the GDR and hopper flow behavior (Table 4).

6. Conclusions

This paper communicates a new method for characterizing the flow properties of cohesive powders under unconfined conditions, i.e., where the cohesive powder is in a dilated state. DEM simulations were fine-tuned by comparison with experimental observations and then used to demonstrate that the GDR measurement (standard deviation of the weight signal recorded by the load cell) is directly proportional to the cohesion of the material. Subsequently, we showed that GDR measurements can be used to define a flow index that predicts flow through small hoppers. This can be useful as a tool for preventing flow problems in processing of cohesive materials, which are a major problem in tablet formulation commonly used in the pharmaceutical, catalysis, and polymer industries.

The method presented here has an important advantage relative to shear cells and related methods. Shear cell measurements are unquestionably useful as a well-established systematic approach for examining incipient yield behavior and related dense-state phenomena. However, for cohesive powders, flow behavior can vary enormously as a function of the degree of consolidation. The ability of the GDR to simultaneously capture flow behavior and allow for the measurement of density under the dilated conditions that are exhibited by the material during processing provides an alternative window of opportunity for developing an enhanced understanding of the

inter-related roles of cohesion and density in determining flow properties.

References

Adams, M.J., Perchard, V., 1985. The cohesive forces between particles with interstitial fluid. Inst. Chem. Eng. Symp. 91, 147–160.

Bagnold, R.A., 1941. The Physics of Blown Sand and Desert Dune. Chapman and Hall, London.

Baxter, J., Abouchakra, H., Tuzun, U., Lamptey, B.M., 2000. A DEM simulation and experimental strategy for solving fine powder flow problems. Trans. IChemE 78, 1019–1025.

Bocquet, L., Ciliberto, S., Crassous, J., 1998. Moisture-induced ageing in granular media and the kinetics of capillary condensation. Nature 396, 735–737.

Brown, R.L., Richards, J.C., 1960. Profile of flow of granules through apertures. Trans. Inst. Chem. Eng. 38, 243–250.

Carr, R.L., 1965. Evaluating flow properties of solids. Chem. Eng. 72, 69–72.

Carstensen, J., 1974. Theory of pharmaceutical systems. In: Heterogeneous Systems, 2nd ed. Academic Press, New York/London, pp. 163–217.

Cundall, P.A., 1971. A computer model for simulating progressive large-scale movements in blocky rock systems. Proc. Symp. Int. Soc. Rock Mech. 2, 129–136.

Dippel, S., Batrouni, G.G., Wolf, D.E., 1996. Collision-induced friction in the motion of a single particle on a bumpy inclined line. Phys. Rev. E 54, 6845.

Doung, N.H., Shen, E., Shinbrot, T., Muzzio, F.J., 2004. Segregation in granular materials and the direct measurement of surface forces using atomic force microscopy. Powder Technol. 145, 69–72.

Faqih, A., Chaudhuri, B., Alexander, A., Muzzio, F., Tomassone. S., 2006. Flow-induced dilation of cohesive granular materials. AIChE, in preparation.

Geldart, D., 1973. Types of gas fluidization. Powder Technol. 7, 285–292.

Hagen, G., Druck, U., Bewegung, D., 1852. Trockenen Sandes. Berl. Monatsb. Akad. Wiss, 35–42.

Hausner, H.H., 1967. Friction conditions in a mass of metal powder. Int. J. Powder Metall. 3, 7–13.

Jenike, A.W., 1964. Storage and flow of solids. Utah. Eng. Exp. Stn. Bull. 123, 1–194.

Johanson, J.R., 1992. The Johanson indicizer system vs. the Jenike shear tester. Bulk Solids Handling 12, 237–240.

Johanson, J.R., 1993. Reliable flow of particulate solids II. Powder Technol., Oslo, 11–32.

Kaye, B.H., Gratton-Liimatainen, J., Lloyd, J., 1995. The effect of flow agents on the rheology of a plastic powder. Part. Syst. Charact. 12, 194–197.

Knowlton, T.A., Carson, J.W., Klinzing, G.E., Yang, W.C., 1994. The importance of storage, transfer and collection. Chem. Eng. Prog. 90, 44–54.

Koeppe, J.P., Enz, K., Kakalios, J., 1998. Phase diagram for avalanche stratification of granular media. Phys. Rev. 58, R4104–R4107.

Lian, G., Thornton, C., Adams, M.J., 1993. A theoretical study of liquid bridge forces between two rigid spherical bodies. J. Colloid Interf. Sci. 161, 138–147.

Luding, S., 1997. Stress distribution in static two dimensional granular model media in the absence of friction. Phys. Rev. 55, 4720.

Maltby, L.P., 1993. Dissertation. Telemark Institute of Technology, Porsgrunn, Norway.

Maltby, L.P., Enstad, J.J., 1993. Uniaxial tester for quality control and flow property characterization of powders. Bulk Solids Handl. 13, 135–139.

McCarthy, J.J., Vargas, W.L., Abatan, A.A., 2001. Discrete characterization tools for cohesive granular material. Powder Technol. 116, 214–223.

McCarthy, J.J., Ottino, J.M., 1998. Particle dynamics simulations: a hybrid technique applied to granular mixing. Powder Technol. 97, 91–99.

Mikami, T., Kamiya, H., Horio, M., 1998. Numerical simulation of cohesive powder behavior in a fluidized bed. Chem. Eng. Sci. 53, 1927–1940.

Moakher, M., Shinbrot, T., Muzzio, F.J., 2000. Experimentally validated computations of flow, mixing and segregation of non-cohesive grains in 3D tumbling blenders. Powder Technol. 109, 58–71.

Nedderman, R.M., Tuzun, U., Savage, S.B., Houlsby, G.T., 1982. The flow of granular materials–discharge rate from hoppers. Chem. Eng. Sci. 37, 1597–1609.

Peleg, M., 1978. Flowability of food powders and methods for its evaluation—a review. J. Food Process Eng. 1, 303–328.

Quintanilla, M.A.S., Valverde, J.M., Castellanos, A., Viturro, R.E., 2001. Looking for self-organized critical behavior in avalanches of slightly cohesive powders. Phys Rev. Lett. 8, 194301–194305.

Rastogi, S., Klinzing, G.E., 1994. Characterizing the rheology of powders by studying dynamical avalanching of powders. Part. Syst. Charact. 11, 453–456.

Reynolds, O., 1885. On the dilatancy of media composed of rigid particles in contact. Phil. Mag. Ser. 20, 469–481.

Ristow, G.W., 1996. Dynamics of granular material in a rotating drum. Europhys. Lett. 34, 263.

Ristow, G., Herrmann, H., 1994. Density patterns in two-dimensional hoppers. Phys. Rev. E 50, R5–R8.

Savage, S.B., Hutter, K., 1989. The motion of a finite mass of granular material down a rough inclined plane. J. Fluid Mech. 199, 177–215.

Schulze, D., 1994. First Particle Technology Forum Denver, pp. 11–16.

Schwedes, J., Schulze, D., 1990. Measurement of flow properties of bulk solids. Powder Technol. 61, 59–68.

Shinbrot, T., Alexander, A., Moakher, M., Muzzio, F.J., 1999. Chaotic granular mixing. Chaos 9, 611–620.

Staniforth, J., 2002. In: Aulton, M.E. (Ed.), Pharmaceutics, 2nd ed. Churchill Livingstone, New York, p. 197.

Strack, O.D.L., Cundall, P.A., 1979. A discrete numerical model for granular assemblies. Geotechnique 29, 47–65.

Sudah, O.S., Arratia, P.E., Alexander, A., Muzzio, F.J., 2005. Simulation and experiments of mixing and segregation in a tote blender. AICHE J. 51, 836–844.

Takeuchi, Y., Yamanoi, K., Endo, Y., Murakami, S., Izumi, K., 2003. Velocities for the dry and wet snow avalanches at Makunosawa valley in Myoko, Japan. Cold Reg. Sci. Technol. 37, 483–492.

Thompson, P.S., Grest, G.S., 1991. Granular flow: friction and the dilatancy transition. Phys. Rev. Lett. 67, 1751–1755.

Walton, O.R., 1992. Numerical simulation of inelastic, frictional particle–particle interactions. Part. Two-Phase Flow 16, 884–911.

Walton, O.R., 1993. Numerical simulation of inclined chute flows of monodisperse, inelastic, frictional spheres. Mech. Mater. 16, 239–247.

Walton, O.R., Braun, R.L., 1986. Viscosity, granular-temperature and stress calculations for shearing assemblies of inelastic, frictional disks. J. Rheol. 30, 949–980.

Wightman, C., Moakher, M., Muzzio, F.J., Walton, O.R., 1998. Use of the discrete element methods to characterize particulate flow and mixing in a rotating and rocking cylinder. AIChE J. 44, 1266–1276.